doi:10.1016/j.jmb.2006.02.006 J. Mol. Biol. (2006) 358, 935–942

JMB

Available online at www.sciencedirect.com

SCIENCE DIRECT®

ELSEVIER

COMMUNICATION

Characterization of the Formation of Amyloid Protofibrils from Barstar by Mapping Residue-specific Fluorescence Dynamics

Samrat Mukhopadhyay[1], Pabitra K. Nayak[1], Jayant B. Udgaonkar[2]* and G. Krishnamoorthy[1]*

[1]*Department of Chemical Sciences, Tata Institute of Fundamental Research, Mumbai 400 005, India*

[2]*National Centre for Biological Sciences, Tata Institute of Fundamental Research Bangalore 560065, India*

**Corresponding authors*

The small protein barstar aggregates at low pH to form soluble oligomers, which can be transformed into fibrillar aggregates at an elevated temperature. To characterize structurally, with residue-specific resolution, the process of amyloid formation of barstar, as well as to monitor the increase in size that accompanies the aggregation process, time-resolved fluorescence anisotropy decay measurements have been introduced as a valuable probe. Seven different single-cysteine-containing mutant forms of barstar were made, to each of which a fluorophore was attached at the thiol group. The rotational dynamics of these seven fluorophores, as well as of the sole intrinsic tryptophan residue in the protein, were determined in the amyloid protofibrils formed, as well as in the soluble oligomers from which the protofibrils arise upon heating. Mapping of the fast rotational dynamics onto the sequence of the protein yields dynamic amplitude maps that allowed identification of the segments of the chain that possess local structure in the soluble oligomer and amyloid protofibrils. The patterns of these maps of the soluble oligomer and protofibrils are seen to be similar; and protofibrils display more local structure than do the soluble oligomers, at all residue positions studied. The observation that transformation from soluble oligomers to protofibrils does not perturb local structure significantly at eight different residue positions, suggests that the soluble oligomers transform directly into protofibrils, without undergoing drastic structural rearrangements.

Keywords: amyloid; Barstar; protein aggregation; time-resolved fluorescence anisotropy; rotational dynamics

Protein misfolding leading to amyloid formation has attracted considerable attention in recent times, due to its involvement in a variety of neurodegenerative diseases such as Alzheimer's, Parkinson's, Huntington's and prion diseases.[1–12] The alternative conformations of amyloidogenic proteins and their multi-step assembly pathways have been under intense scrutiny.[11] The notion that protein aggregation is a cause, rather than an effect, of neurodegeneration has undergone numerous experimental tests.[9] Hence, understanding the mechanism of the conformational change by which soluble functional proteins transform into insoluble aggregates is critical to obtaining an understanding of the molecular basis of these diseases. Transformation of a native protein into fibrils appears to occur *via* steps involving soluble oligomers. Structures formed late during the transformation include the larger precursors termed protofibrils. Protofibrils, which consist of arrays of protein molecules rich in β-structure, have been implicated as the toxic species responsible for cell dysfunction and neuronal loss in Alzheimer's

Present address: S. Mukhopadhyay, Department of Molecular Biology, MB-19. The Scripps Research Institute, 10550 N. Torrey Pines Road, La Jolla, CA 92037, USA.

Abbreviations used: AFM, atomic force microscopy; IAEDANS, 5-((((2-iodoacetyl) amino)-ethyl)amino)-naphthalene-1-sulfonic acid.

E-mail addresses of the corresponding authors: jayant@ncbs.res.in; gk@tifr.res.in

disease and other protein aggregation diseases.[9] For a proper understanding of the role of soluble oligomers in amyloid protofibril or fibril formation, it is important to obtain residue-specific structural information of the aggregation process.

Recently, solid-state NMR methods[13] as well as X-ray crystallographic methods,[14,15] have provided considerable insight into structures of amyloid fibrils. The same peptide may form fibrils of different morphologies having different underlying molecular structures, as seen in the case of the Aβ peptide.[13] The cross-β structural motif, in which continuous β-sheets are formed with β-strands running perpendicular to the long axis of the fibrils, is a defining characteristic, but the β-strands may adopt either parallel or antiparallel arrangements in the case of the Aβ peptide, depending on its length.[10] A parallel β-helix, which is primarily a β-sheet structure with the proper cross-β-orientation, may also be adopted.[16] Nevertheless, there are some striking, albeit gross, structural similarities between fibrils formed by different proteins,[17] as well as between the soluble precursors from which the fibrils arise.[18] To obtain an understanding of how polypeptide sequence and length determine general features of structural organization within fibrils, and of how different fibrillization conditions affect fibril morphology, it is necessary to study the process of amyloid formation using different proteins.

The ability to undergo amyloid-like fibrous aggregation is not restricted to proteins associated with amyloid diseases; many proteins are able to aggregate *in vitro* into fibrils under special environmental conditions.[5,12] One advantage of studying aggregation using proteins whose folding and unfolding pathways have been well-characterized is that the folding and unfolding studies often lead to a better understanding of a key early step in protein misfolding and aggregation, which is the conformational change that the protein undergoes when partially destabilized. An archetypal model protein for folding studies is the 89 amino acid residue protein barstar, which is a natural inhibitor of barnase, an extracellular endoribonuclease in *Bacillus amyloliquefaciens*. Native barstar is monomeric (10.1 kDa) with three parallel α-helices packed against a three-stranded parallel β-sheet, and with a more poorly defined short helix (Figure 1(a)).[19] At low pH, barstar unfolds partially and reversibly to a molten globule-like A-form,[20–24] which possesses 60% of the secondary structure present in the native protein, but is devoid of well-defined tertiary interactions. Sedimentation velocity measurements have indicated that it is a soluble aggregate with an apparent molecular mass of about 150 kDa.[21] Characterization of the A-form using NMR spectroscopy has revealed that the protein forms symmetrical aggregates (containing 15 or 16 molecules) in which the N-terminal segment, anchored to the aggregated core comprised of C-terminal segments, does not take part in the aggregation and exhibits large amplitude-independent motion.[24] At higher temperatures, the A-form has been shown to transform into amyloid fibrils.[25] Our atomic force microscopy (AFM) images reveal the presence of short and curved protofibrils, with a diameter of ≈10 nm and a length of 100–200 nm (Figure 1(b)). These protofibrils transform into long and straight fibrils in a very slow process, which takes one to two days at room temperature (Figure 1(c)). A major attraction for using barstar as a model protein for studying amyloid formation is its potential utility for understanding how a soluble oligomer such as the A-form is transformed into protofibrils and fibrils.

Fluorescence methods of various levels of sophistication have proven to be of much use in unraveling the structural characteristics of amyloid

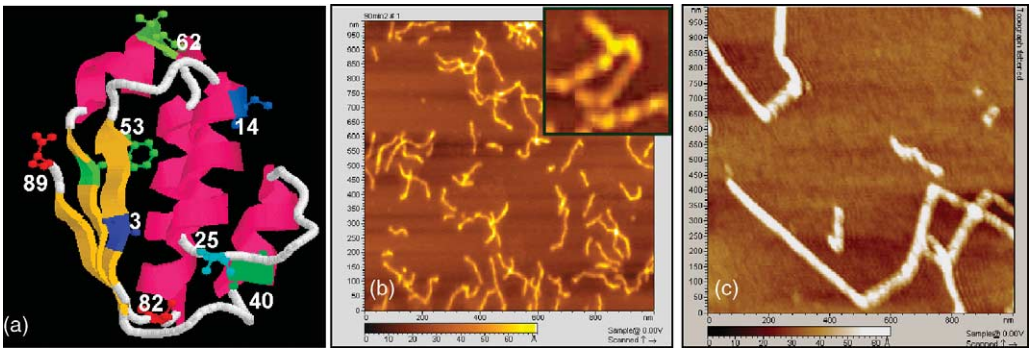

Figure 1. (a) Structure of barstar indicating the core Trp53 and sites of single Cys mutations (drawn from PDB). Each single cysteine-containing mutant protein was labeled at its thiol using IAEDANS, as described in Supplementary Data. (b) AFM image of protofibrils from fluorescently labeled barstar [Cys62-AEDANS]. The inset shows a magnified image. The protein sample (50 μM at pH 2.7) was incubated at 70 °C for 2 h. (c) AFM image of matured fibrils from fluorescently labeled barstar [Cys62-AEDANS]. The protein sample (50 μM at pH 2.7) was incubated at 70 °C for 2 h, and then at 25 °C for 48 h. For each AFM image, an aliquot of the protein sample was transferred (after diluting 1:10 (v/v) with pH 2.7 buffer) onto a freshly cleaved mica surface. After incubating for 5 s, the mica surface was rinsed with 2×200 μl of water and dried under a stream of N_2 for 45 min before it was scanned. The AFM image was obtained with a PicoPlus AFM instrument (Molecular Imaging Inc., Arizona, USA) operating in non-contact mode using NCL cantilevers (Nanosensors Inc., Switzerland) with a resonance frequency of 165 kHz and a force constant ∼50 N/m.

fibrils.[26–29] For example, residue-specific steady-state fluorescence intensity measurements have been particularly effective for characterizing the amyloid core of the yeast prion protein.[26] Steady-state fluorescence anisotropy methods have been of use in the case of the islet amyloid peptide.[27,28] Time-resolved fluorescence measurements have been shown to be useful in the early detection of Alzheimer β-peptide.[29] Surprisingly, the power of time-resolved fluorescence methods, which have proven to be so useful in providing both global and residue-specific structural information on protein folding mechanisms,[30–32] has not been exploited in the structural study of protein aggregation.

Unlike steady-state fluorescence measurements, time-resolved fluorescence anisotropy decay measurements provide insights into the global dynamics (tumbling), and into the local dynamics of the fluorophores and their surroundings.[33–37] The intrinsic (time zero) fluorescence anisotropy, r_0, can decay by local (fast) rotation of the fluorophore, which is characterized by rotational correlation time ϕ_{fast}, as well as by global (slow) motion of the entire molecule, which is characterized by the global rotational correlation time ϕ_{slow}:

$$r(t) = r_0[\beta_{fast} \exp(-t/\phi_{fast}) + \beta_{slow} \exp(-t/\phi_{slow})] \quad (1)$$

$r(t)$ is the dynamic (time-dependent) fluorescence anisotropy; ϕ_{slow} is related to the size (V) of the aggregate by the Stokes–Einstein–Debye equation in which η is the viscosity:

$$\phi_{slow} = \eta V/kT \quad (2)$$

The amplitude of the local motion (β_{fast}) indicates the rotational freedom (or the "degree of orientational constraint") of the probe.[38] In this work, β_{fast}, which is related to the flexibility of the probe, is the main structural parameter used to bring out the information on the internal organization in both oligomers and protofibrils. The other parameters, including both the correlation times, are largely insensitive to the location of the probe (see later). Here, measurements of residue-specific fluorescence dynamics have been shown to be an effective approach to characterize, at the individual residue level, the formation of protofibrils from barstar.

Residue-specific fluorescence dynamics of native barstar

Seven single-cysteine-containing (at positions 3, 14, 25, 40, 62, 82 and 89) mutant forms of barstar were made, and each was labeled with the thiol-active fluorescent probe, 5-((((2-iodoacetyl) amino)-ethyl)amino)naphthalene-1-sulfonic acid (IAEDANS) whose fluorescence lifetime is long ($\geq$10 ns). Additionally, the single tryptophan residue at position 53 was used as an intrinsic fluorescence probe. In the native form, fluorescence anisotropy decay kinetics of all the labeled proteins showed similar long rotational correlation times (4.0($\pm$1.0) ns), which agree well with the size of native barstar (hydrodynamic radius is 1.7($\pm$0.4) nm), as reported in our earlier studies.[37] An additional short rotational correlation time (ϕ_{fast} < 1 ns) was observed, whose amplitude (β_{fast}) is indicative of the extent of angular diffusion of the probe (Table 1) according to the wobbling-in-cone model (Figure 2).[38] Different positions showed varied amplitudes for this fast motion, which can be correlated with the native structure of barstar. Residue 3 is buried in the core and the probe attached to Cys3 has smaller amplitude of local motion, whereas, residue 89 is completely exposed and the probe attached to Cys89 has the most significant amplitude of local motion. Trp53 is completely buried in the hydrophobic core, and does not display any local motion, as revealed by a single-exponential decay in the fluorescence anisotropy.[37]

Residue-specific dynamics in soluble oligomers (A-form)

Upon a jump from pH 8 to pH 2.7, the long component in the time-resolved decay of the fluorescence anisotropy of barstar increases from ~4.5 ns (pH 8.0) to >100 ns (pH 2.7). This can be ascribed to the formation of large oligomeric assemblies, since the aggregate size is related to the long rotational correlation time (equation (2)). Aggregation begins in less than 1 min, and continues to occur for several hours. For 50 μM protein, a sharp increase in ϕ_{slow} (thus in size) was observed till about 0.5 h (Figure 3). After 2 h, the rate of increase essentially levels off, and the rotational correlation time is found to range between 100 ns and 130 ns, indicative of the tumbling of an apparent molecular mass of 150–160 kDa.

Interestingly, different positions show widely varying amplitudes for the fast motion, indicating that the structure of the A-form is specific (Table 1). We introduce the terms structure gain (for the decrease in the amplitude of the fast motion) and structure loss (for the increase in the amplitude of the fast motion) during pH-induced oligomerization of barstar. In the A-form, the large amplitude fast motion of residues 3 and 14 indicates that the N terminus is unstructured in the A-form; in contrast, residues 82 and 89 display low-amplitude fast motion suggesting that the C-terminal region is more structured in the A-form. The most significant structure loss was observed for residue 3, indicating that the N terminus is unstructured and not involved in the aggregation. This observation corroborates our earlier NMR-data.[24] The dynamics of the N terminus residues 3 and 14 resemble closely that of the unfolded chain in showing a three-exponential decay of fluorescence anisotropy yielding a long component ($\approx$100 ns) and two well-resolved fast motions, namely, segmental and local. The middle region appears to be flexible in the A-form: Trp53 shows significant fast motion, unlike

Table 1. Typical parameters associated with time-resolved fluorescence measurements

Position	Native protein				Soluble oligomer (A-form)				Protofibrils				
	ϕ_{slow} (ns) (β_{slow})	ϕ_{fast} (ns) (β_{fast})	τ_m [a] (ns)	λ_{max} [b] (nm)	ϕ_{slow} (ns) (β_{slow})	ϕ_{fast} (ns) (β_{fast})	τ_m [a] (ns)	λ_{max} [b] (nm)	ϕ_{slow} (ns) (β_{slow})	ϕ_{fast} (ns) (β_{fast})	τ_m [a] (ns)	λ_{max} [b] (nm)	k_q [c] ($\times 10^8$ M^{-1} s^{-1})
3	4.2 (0.81)	0.7(0.19)	12.7	494	>100 (0.54)	2.4 (0.20) 0.4 (0.26)	14.6	487	>200 (0.68)	1.8 (0.18) 0.2 (0.14)	13.1	485	1.7
14	4.7 (0.68)	0.7(0.32)	10.5	496	>100 (0.60)	4.2 (0.20) 0.5 (0.20)	12.6	486	>200 (0.82)	1.4 (0.18)	12.8	481	1.1
25	3.8 (0.70)	0.4(0.30)	8.3	496	120 (0.81)	1.9 (0.19)	13.1	485	>200 (0.90)	1.0 (0.10)	12.2	481	0.9
40	4.8 (0.75)	0.6(0.25)	12.8	492	124 (0.88)	1.7 (0.12)	15.6	475	>200 (0.93)	2.1 (0.07)	14.7	475	0.4
53[d]	4.3 (1.0)	–	4.8	331	>50 (0.55)	0.5 (0.45)	2.3	340	>50 (0.63)	0.6 (0.37)	2.4	339	4.4
62	3.5 (0.62)	0.4(0.38)	10.6	496	135 (0.82)	2.1 (0.18)	14.3	483	>200 (0.88)	1.5 (0.12)	12.5	483	0.4
82	4.3 (0.70)	0.4(0.30)	12.8	493	111 (0.89)	2.7 (0.11)	13.9	477	>200 (0.92)	2.1 (0.08)	14.4	473	0.4
89	3.5 (0.52)	0.3(0.48)	8.6	497	139(0.84)	3.2 (0.16)	13.9	476	>200 (0.83)	1.3 (0.17)	13.9	474	0.6

Errors in $\phi_{fast} \pm 0.2$ ns; $\beta_{fast} \pm 0.02$; $\phi_{slow} \pm 20$ ns; $\beta_{slow} \pm 0.02$; τ_m (mean fluorescence lifetime) ± 0.01 ns. Data were collected at 460 nm emission wavelength after incubating the labeled proteins (50 μM) at pH 2.7 at room temperature (24(±1) °C) for 2 h for soluble oligomers and at 70 °C for 2 h for protofibrils.

[a] Mean fluorescence lifetime obtained by magic angle measurements.

[b] Emission maxima.

[c] k_q is the bimolecular quenching constant; $\tau_0/\tau = 1 + k_q\tau_0[Q]$. τ is the fluorescence lifetime at a quencher concentration [Q], $\tau = \tau_0$ at [Q] = 0.

[d] Corresponds to Trp fluorescence. It should be pointed out that the fluorescence anisotropy decay of Trp in aggregates does not allow us to obtain the correct estimate of the long rotational correlation time due the short fluorescence lifetime of Trp.

in the native form, where it shows no fast motion because it is completely buried. The mean fluorescence lifetime of Trp53 is also much shorter (2.3 ns) compared to that in the native form (4.8 ns), indicating a much greater solvent-exposure of Trp53 in the A-form. This result is corroborated by the observation that the fluorescence emission maximum of Trp53 in the A-form is red-shifted with respect to that in the native state (Table 1). The residue-specific time-resolved fluorescence anisotropy decay measurements therefore allow the construction of a dynamic amplitude map that illustrates the structural fine-points in the A-form. The order of flexibility in the A-form of barstar can be seen from the map shown in Figure 4(b).

Residue-specific dynamics in protofibrils

The A-form of barstar is transformed into protofibrils (Figure 1(b)) by incubation at 70 °C.[25] A significant increase in the long (global) rotational correlation time (>200 ns) is seen during the transformation to protofibrils. This value, which represents the higher limit of our measurements, indicates the formation of structures of very large size. Global tumbling correlation times of structures of 10 nm diameter and several hundred nanometers long are expected to be microseconds and beyond.

In the protofibrils, the amplitude associated with the shorter correlation time, β_{fast} which is the main structural parameter (Figure 4), is diminished for all the residues except for residue 89 (Table 1). Thus all residues, except residue 89, show structure gain on going from the soluble oligomeric A-form to the protofibrils, as shown by the decrease in the values of β_{fast} (Table 1). This observation points out the formation of a much more ordered aggregate upon fibrillation. Interestingly, two out of the three β-sheets, which were originally present in the native form, appear to have lost some structural ordering, as indicated by large amplitude, fast rotation found in residue 3 (β-1) and residue 53 (β-2). The region around residue 25 appears to be more structured compared to those around residues 3 and 14, but far less structured compared to that around residue 40 (Table 1 and Figure 4(a)). The dynamic amplitude map constructed for protofibrils is shown in Figure 4(b).

The dynamic amplitude map for the protofibrils is very similar to that of the soluble oligomers, the A-form (see above), except in the overall decrease in values of β_{fast}, suggesting that the A-form may act as the precursor for protofibrils. Thus, the structure in the fibrils seems to be a more consolidated form of that in the A-form oligomers. This observation makes it unlikely that the A-form transforms into protofibrils by first undergoing drastic internal structural reorganization, because the dynamic amplitude maps would then not be expected to be so similar. The possibility that the similarity of the two dynamics maps for the A-form and the protofibrils may be due to the presence of large levels of the A-form in the samples of protofibrils

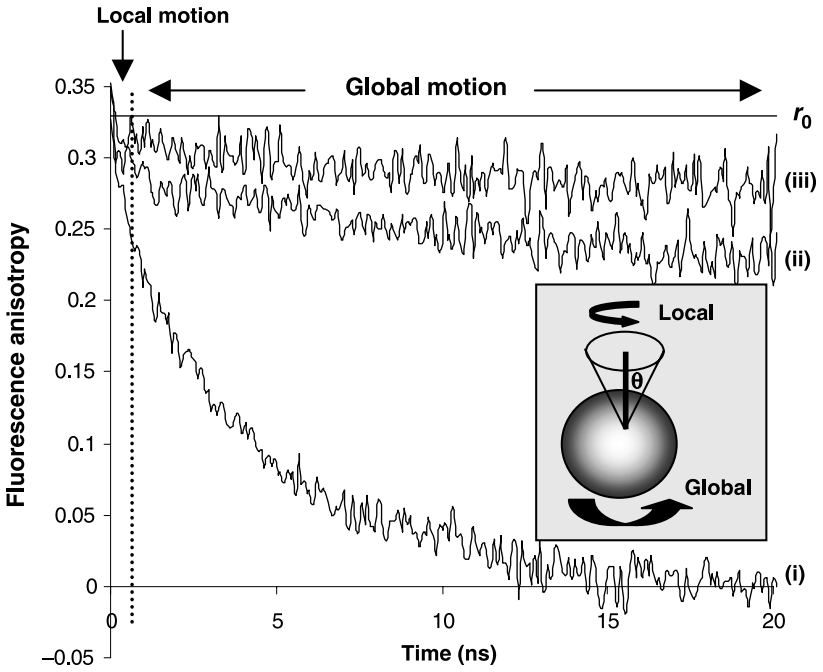

Figure 2. Time-resolved fluorescence anisotropy decay of barstar [Cys-40-AEDANS] in native form (i), A-form (ii) and protofibrils (iii). r_0, the time-zero fluorescence anisotropy of IAEDANS, was measured separately by immobilizing the probe in glycerol. Time-resolved fluorescence decay measurements were made using a high repetition rate picosecond laser (frequency doubled Ti-sapphire laser, Tsunami from Spectra-Physics Inc., USA) coupled to a time-correlated, single-photon counting (TCSPC) setup.[30–32] The width (FWHM) of the instrument response function was ~40 ps. The inset shows the wobbling-in-cone model (θ is the cone-angle) to illustrate the local and global rotational motions of fluorophores linked covalently to macromolecules.[38]

can be ruled out because no significant amounts of soluble oligomers are seen in the AFM images of protofibrils (Figure 1(b)). AFM images, of which Figure 1(b) is typical, also show that no amorphous aggregates co-exist with the protofibrils.

No detectable change in fluorescence dynamics, for several hours after the formation of protofibrils, was observed at any of the eight locations. After a long incubation period, we had observed, by AFM imaging, the transformation of protofibrils to fibrils having linear structures (Figure 1(c)). Thus, we infer that the internal structure of protofibrils and fibrils are very similar to each other.

We feel it is essential to address the following important issues related to the present study. (i) The organic probe used in this study may induce additional structural changes in the protein molecule and whether, by doing so, it might affect the fibrillation process. There are, however, several observations that suggest that this is not the case: (a) all labeled and unlabeled proteins assemble to form soluble oligomers (the A-form) and protofibrils like wild-type barstar under similar conditions. (b) All of them form soluble oligomers (the A-form) of comparable size, as evident from the long rotational correlation time, ϕ_{slow}. (c) Similar results are obtained by using a different thiol-active fluorescent probe, namely acrylodan (data not shown). (d) The data for the A-form are corroborated by NMR data obtained using wild-type barstar.[24] Of course, at this stage, it is difficult to rule out completely the minor effects of probe labeling. (ii) We have compared the dynamics of AEDANS at seven different locations with that of Trp53, although the properties of these two probes are, of course, significantly different. Since the linker arm of Trp is much shorter than that of AEDANS adduct, the amplitude associated with the fast rotational correlation time should be smaller in the case of Trp53 when the flexibilities are similar. But we observe an increase in the amplitude at Trp53 when compared to Cys40 and Cys62, indicating that Trp53 is much more flexible. It is possible that Trp53 resides in a flexible loop connecting two segments of the chain participating in the aggregate core. (iii) We have measured the fluorescence emission of the AEDANS adduct at 460 nm (Table 1) as well as at 530 nm (Supplementary Data Table S1). The fluorescence emission of AEDANS is very sensitive towards its local environment; thus, the emission at 460 nm probes the population of protein molecules in which the AEDANS is buried, while emission at 530 nm is biased towards the population of protein molecules

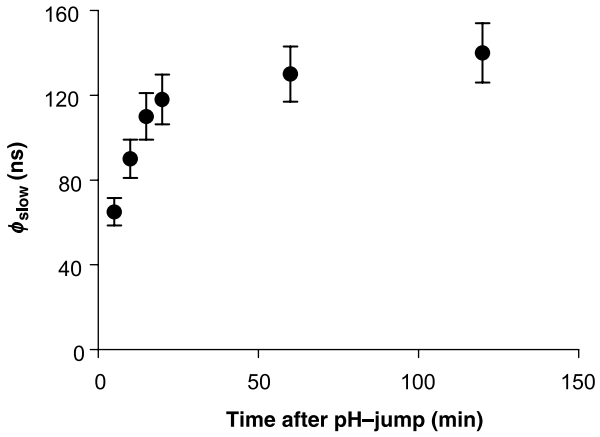

Figure 3. Kinetics of aggregation leading to the formation of soluble oligomers (A-form) of barstar. Time-course of change in the slow rotational correlation time (ϕ_{long}), following a pH jump from 8 to 2.7, of fluorescently labeled barstar [Cys62-AEDANS] (50 μM, at 24(± 1) °C).

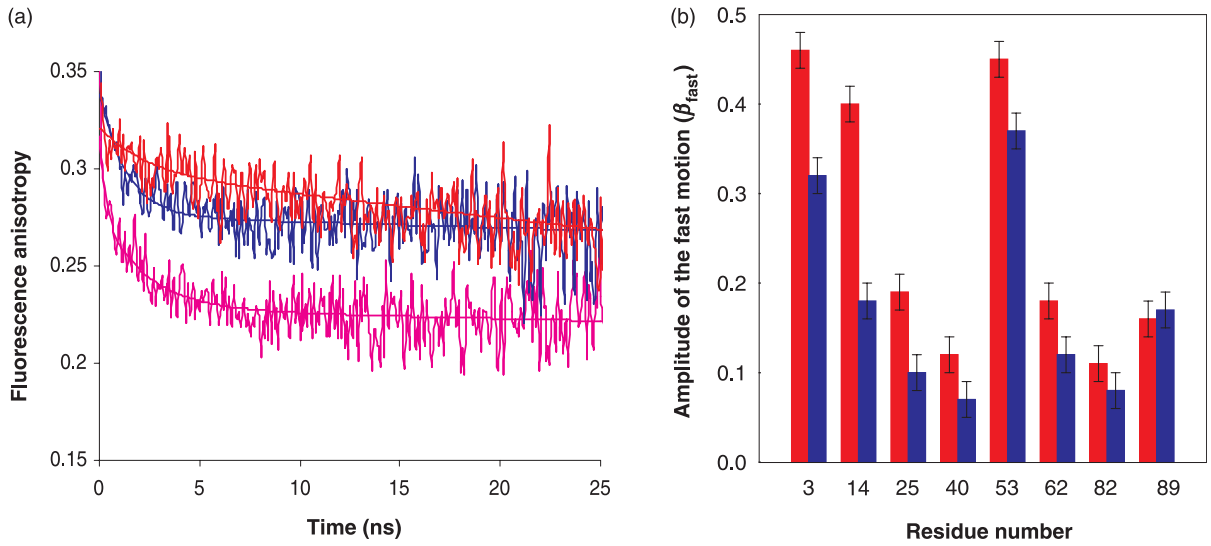

Figure 4. (a) Typical profiles of fluorescence anisotropy decay of barstar in protofibrils with simulated fits (continuous lines). AEDANS labeled at Cys3, pink; at Cys14, blue; and at Cys40, red. (See Table 1 for typical parameters.) Smooth lines were simulated with the parameters shown in Table 1. The samples were excited at 418 nm and emissions were collected at 460 nm (see Supplementary Data for more information). (b) Dynamic amplitude map (representing the amplitude, β_{fast}, of the short rotational correlation time) of barstar in the A-form (red) and protofibrils (blue).

in which the AEDANS is exposed. Hence, we see that the values of β_{fast} are consistently lower when determined from data collected at 460 nm than when determined from data collected at 530 nm. The pattern in the values of β_{fast} apparent in the dynamic amplitude maps constructed from data collected at the two wavelengths is essentially unchanged. (iv) We have excited AEDANS-labeled barstar at 418 nm, which is on the far red side of the absorbance peak (337 nm). The use of the longer excitation wavelength provides higher initial intrinsic anisotropy ($[r_0]_{418\ nm}=0.33$) than what would have been provided by use of a wavelength on the blue side of the absorbance peak ($[r_0]_{307\ nm}=0.22$), which allows us to detect smaller changes in the dynamics. Furthermore, the choice of the excitation wavelength in such studies is, in general, restricted by the availability of suitable laser sources, as in this case. Fortunately, the absorbance spectrum of AEDANS is not very sensitive to its environment. Table 1 also shows the site-specific value of the wavelength of maximum emission (λ_{max}) of the AEDANS adduct. While the pattern of λ_{max} is similar to that of β_{fast} (Table 1), there are a few discrepancies. It is likely that β_{fast} is a more reliable structural parameter when compared to λ_{max}.

Dynamic quenching corroborates the time-resolved fluorescence anisotropy results

Time-resolved fluorescence anisotropy carries the information on the extent of angular diffusion of the probe. Although it is possible that a probe having large internal motion may be buried and solvent-inaccessible, it is far more likely that the residues that have larger angular diffusion (large amplitude local motion, β_{fast}) will be exposed to the aqueous phase and, consequently, will be expected to demonstrate efficient dynamic quenching. For protofibrils, we observe that the pattern of dynamic quenching by acrylamide (solvent-exposure) is similar to that of dynamic fluorescence anisotropy (local motion, β_{fast}). Here again, we find that the fluorescence of Trp53 is quenched extensively, indicating that it is highly exposed. Thus, the values of the bimolecular quenching constant, k_q (which is related to the solvent-exposure), in protofibrils, appear to correlate closely with the time-resolved fluorescence anisotropy data (Table 1).

Structural insights into the aggregation process

The dynamic amplitude map points out the regions that are involved in the protofibrillar assembly. It would appear that the N terminus is not involved, because of fewer hydrophobic residues and because of the presence of more positively charged residues at pH 2.7. The region comprising residues 40 to 82 appears more prone to self-assembly, presumably because of the presence of more hydrophobic and fewer charged residues. Hydrophobic interactions appear to play a major role in defining amyloid structure.

For many proteins, partially unfolded molten globule forms appear to be the precursors for amyloid aggregation.[5,6] In this study, it has been possible to obtain residue-specific information on the amyloid protofibrils, and on the soluble oligomer (A-form), from which they appear to arise. An important point to address is whether the A-form is on-pathway or off-pathway during the fibrillation process. The pattern of structure, as displayed in the dynamic amplitude map is similar in the A-form and protofibrils (Figure 4(b)), and all

the residue positions demonstrated structure gain during the process of transformation from the A-form to protofibrils. Since formation of amyloid structure from soluble precursors is expected to be progressive and accumulative, the similarity between the dynamic amplitude maps of the A-form and protofibrils makes it unlikely that the A-form is off-pathway to the direct fibrillation process. Moreover, in higher magnification AFM images, small spherical beads are observed in protofibrils (Figure 1(b), inset). These beads are likely to represent spherical oligomers (A-form) annealed into a pearls-on-a-string morphology in the protofibrils.

Conclusion

In this study, it has been possible to obtain residue-specific information on the protofibrils, and on the soluble oligomers (A-form), which appear to be their precursor. Characterization of the rotational dynamics at eight different positions on the polypeptide chain indicates that the transformation of the A-form into amyloid does not alter the local structure significantly at these positions. Hence, it appears that the internal structure of the soluble oligomers is largely preserved during this transformation. It is anticipated that the novel dynamic fluorescence-based method, introduced here for the study of amyloid aggregation, will allow us to interrogate the initial steps that determine the mechanism of amyloid formation.

Acknowledgements

We thank Kalyan Sinha for donating some of the protein preparations used in this study, and Professor N. Periasamy (TIFR, Mumbai) for providing the software for the fluorescence decay analysis.

Supplementary Data

Supplementary data associated with this article can be found, in the online version, at doi:10.1016/j.jmb.2006.02.006

References

1. Ramos, C. H. I. & Ferreira, S. T. (2005). Protein folding, misfolding and aggregation: evolving concepts and conformational diseases. *Protein Pept. Letters*, **12**, 213–222.
2. Dimakopoulos, A. C. (2005). Protein aggregation in Alzheimer's disease and other neoropathological disorders. *Curr. Alzheimer Res.* **2**, 19–28.
3. Wetzel, R. (ed.) (1999). Amyloid, prions, and other protein aggregates. In *Methods in Enzymology*, vol. 309, Academic Press, San Diego, CA.
4. Cox, D. L., Lashuel, H., Lee, K. Y. C. & Singh, R. R. P. (2005). The materials science of protein aggregation. *Mat. Res. Soc. Bull.* **30**, 452–458.
5. Uversky, V. N. & Fink, A. L. (2004). Conformational constraints for amyloid fibrillation: the importance of being unfolded. *Biochim. Biophys. Acta*, **1698**, 131–153.
6. Jahn, T. Radford, S.E. (2004). The beta sheet conformation and disease. In *Amyloid Proteins* (Sipe, J., ed.), Wiley VCH, Weinheim, pp. 173–211.
7. Miranker, A. D. (2004). Unzipping the mysteries of amyloid fiber formation. *Proc. Natl Acad. Sci. USA*, **101**, 4335–4336.
8. Dobson, C. M. (2003). Protein folding and misfolding. *Nature*, **426**, 884–890.
9. Caughey, B. & Lansbury, P. T. (2003). Protofibrils, pores, fibrils, and neurodegeneration: separating the responsible protein aggregates from the innocent bystanders. *Annu. Rev. Neurosci.* **26**, 267–298.
10. Tycko, R. (2004). Progress towards a molecular-level structural understanding of amyloid fibrils. *Curr. Opin. Struct. Biol.* **14**, 96–103.
11. Kelly, J. W. (1998). The alternative conformations of amyloidogenic proteins and their multi-step assembly pathways. *Curr. Opin. Struct. Biol.* **8**, 101–106.
12. Dobson, C. M. (1999). Protein misfolding, evolution and disease. *Trends Biochem. Sci.* **24**, 329–332.
13. Petkova, A. T., Leapman, R. D., Guo, Z., Yau, W.-M., Mattson, M. P. & Tycko, R. (2005). Self-propagating, molecular-level polymorphism in Alzheimer's β-amyloid fibrils. *Science*, **307**, 262–265.
14. Nelson, R., Sawaya, M. R., Balbirnie, M., Madsen, A. Ø., Riekel, C., Grothe, R. & Eisenberg, D. (2005). Structure of the cross-β spine of amyloid-like fibrils. *Nature*, **435**, 773–778.
15. Makin, O. S., Atkins, E., Sikorski, P., Johansson, J. & Serpell, L. C. (2005). Molecular basis for amyloid fibril formation and stability. *Proc. Natl Acad. Sci. USA*, **102**, 315–320.
16. Wille, H., Michelitsch, M. D., Guénebaut, V., Supattapone, S., Serban, A., Cohen, F. E. *et al*. (2002). Structural studies of the scrapie prion protein by electron crystallography. *Proc. Natl Acad. Sci. USA*, **99**, 3563–3568.
17. O'Nuallain, B. & Wetzel, R. (2002). Conformational Abs recognizing a generic amyloid fibril epitope. *Proc. Natl Acad. Sci. USA*, **99**, 1485–1490.
18. Kayed, R., Head, E., Thompson, J. L., McIntire, T. M., Milton, S. C., Cotman, C. W. & Glabe, C. G. (2003). Common structure of soluble amyloid oligomers implies common mechanism of pathogenesis. *Science*, **300**, 486–489.
19. Lubienski, M. J., Bycroft, M., Freund, S. M. V. & Fersht, A. R. (1994). 3-Dimensional solution structure and C-13 assignments of barstar using nuclear-magnetic-resonance spectroscopy. *Biochemistry*, **33**, 8866–8877.
20. Khurana, R. & Udgaonkar, J. B. (1994). Equilibrium unfolding studies of barstar: evidence for an alternative conformation which resembles a molten globule. *Biochemistry*, **33**, 106–115.
21. Khurana, R. (1995) pH dependence of the conformation of the small protein barstar, PhD thesis, Mumbai University, Mumbai, India.
22. Swaminathan, R., Periasamy, N., Udgaonkar, J. B. & Krishnamoorthy, G. (1994). Molten globule-like conformation of barstar: a study by fluorescence dynamics. *J. Phys. Chem.* **98**, 9270–9278.
23. Khurana, R., Hate, A. T., Nath, U. & Udgaonkar, J. B. (1995). pH dependence of the stability of barstar to

chemical and thermal denaturation. *Protein Sci.* **4**, 1133–1144.
24. Juneja, J., Bhavesh, N. S., Udgaonkar, J. B. & Hosur, R. V. (2002). NMR identification and characterization of the flexible regions in the 160 kDa molten globule-like aggregate of barstar at low pH. *Biochemistry,* **41**, 9885–9899.
25. Gast, K., Modler, A. J., Damaschun, H., Kröber, R., Lutsch, G., Zirwer, D. *et al*. (2003). Effect of environmental conditions on aggregation and fibril formation of barstar. *Eur. Biophys. J.* **32**, 710–723.
26. Krishnan, R. & Lindquist, S. L. (2005). Structural insights into a yeast prion illuminate nucleation and strain diversity. *Nature*, **435**, 765–772.
27. Koo, B. W. & Miranker, A. D. (2005). Contribution of the intrinsic disulfide to the assembly mechanism of islet amyloid. *Protein Sci.* **14**, 231–239.
28. Padrick, S. B. & Miranker, A. D. (2002). Islet amyloid: phase partitioning and secondary nucleation are central to the mechanism of fibrillogenesis. *Biochemistry,* **41**, 4694–4703.
29. Allsop, D., Swanson, L., Moore, S., Davies, Y., York, A., El-Agnaf, O. M. A. & Soutar, I. (2001). Fluorescence anisotropy: a method for early detection of Alzheimer β-peptide (Aβ) aggregation. *Biochem. Biophys. Res. Commun.* **285**, 58–63.
30. Sridevi, K., Lakshmikanth, G. S., Krishnamoorthy, G. & Udgaonkar, J. B. (2004). Increasing stability reduces conformational heterogeneity in a protein folding intermediate ensemble. *J. Mol. Biol.* **337**, 699–711.
31. Lakshmikanth, G. S., Sridevi, K., Krishnamoorthy, G. & Udgaonkar, J. B. (2001). Structure is lost incrementally during the unfolding of barstar. *Nature Struct. Biol.* **8**, 799–804.
32. Sridevi, K., Juneja, J., Bhuyan, A. K., Krishnamoorthy, G. & Udgaonkar, J. B. (2000). The slow folding reaction of barstar: the core tryptophan region attains tight packing before substantial secondary and tertiary structure formation and final compaction of the polypeptide chain. *J. Mol. Biol.* **302**, 479–495.
33. Lakowicz, J. R. (1999). *Principles of Fluorescence Spectroscopy*, Plenum Press, New York.
34. Saxena, A., Udgaonkar, J. B. & Krishnamoorthy, G. (2005). Protein dynamics and protein folding dynamics revealed by time-resolved fluorescence. In *Applications of Flourescence Spectroscopy* (Hof, M., Hutter, R. & Fidler, V., eds), Springer, New York, pp. 163–179.
35. Krishnamoorthy, G. (2003). Fluorescence spectroscopy in molecular description of biological processes. *Ind. J. Biochem. Biophys.* **40**, 147–159.
36. Lakshmikanth, G. S. & Krishnamoorthy, G. (1999). Solvent-exposed tryptophans probe the dynamics at protein surfaces. *Biophys. J.* **77**, 1100–1106.
37. Rami, B. R., Krishnamoorthy, G. & Udgaonkar, J. B. (2003). Dynamics of the core tryptophan during the formation of a productive molten globule intermediate of barstar. *Biochemistry,* **42**, 7986–8000.
38. Kinoshita, K. J., Kawato, S. & Ikegami, A. (1977). A theory of fluorescence polarization decay in membranes. *Biophys. J.* **20**, 289–305.

Edited by P. T. Lansbury Jr

(Received 8 September 2005; received in revised form 18 December 2005; accepted 2 February 2006)
Available online 20 February 2006